Available online at www.sciencedirect.com

ScienceDirect

Procedia CIRP 118 (2023) 839–844

www.elsevier.com/locate/procedia

16th CIRP Conference on Intelligent Computation in Manufacturing Engineering, CIRP ICME '22, Italy

Effects of fibre misalignment on the stability of double-curved composites

Jan-Lukas Stüven[a,*], Sebastian Heimbs[a], Carsten Schmidt[b]

[a] *Technische Universität Braunschweig, Institute of Aircraft Design and Lightweight Structures, Ottenbecker Damm 12, 21684 Stade, Germany*
[b] *Leibniz Universität Hannover, Institute of Production Engineering and Machine Tools, Ottenbecker Damm 12, 21684 Stade, Germany*

* Corresponding author. Tel.: +49 4141 77638-208; *E-mail address:* j.stueven@tu-braunschweig.de

Abstract

In the context of developing a novel technology for the automated production of continuously draped preforms, the effects of fibre misalignment on the stability of double-curved, unidirectional plies are investigated. The critical buckling stress as well as correlations with geometric parameters are analysed numerically using a parametric finite element model. For this purpose, a test program is conducted comprising various geometric configurations. The results provide a foundation for extending the investigation to laminates and indicate significant dependencies of the critical buckling stress on the curvature, length-to-thickness ratio and fibre angle.

Keywords: Fibre misalignment; Stability; Buckling; Curvature; Finite element analysis

1. Introduction

Fibre-reinforced plastics (FRP) are often used in lightweight structures due to their excellent weight-specific properties. Rotor blades, e.g. for wind or tidal turbines, constitute typical applications for FRP and are commonly manufactured by infusing dry, textile preforms consisting of multiple, manually draped layers with a polymeric matrix [1]. As a result of the complex, double-curved blade geometries, automated preform production technologies are not yet state of the art. However, they are highly desirable as to improve the preform quality by reducing the extent and severity of manufacturing defects such as fibre misalignment. In this context, being able to quantify and understand the effects of defects on mechanical properties allows for the reduction of safety factors and optimisation of the manufacturing process, thereby achieving a more efficient design and gaining competitive advantages [2].

Fibre misalignment can occur for various reasons and may be categorised as stochastic or systematic. The former type primarily concerns the orientation of fibres in as-delivered textiles, which can be described adequately using a Gaussian distribution [3]. Standard deviations differ throughout published studies, e.g. 0.7°-1.9° [3], 0.8°-0.9° [4], 1.2° [5], 1.5° [6], 3° [7]. The effect of stochastic fibre misalignment on mechanical properties decreases with increasing ply count and number of intended fibre orientations as it becomes more likely that negative effects resulting from the misalignment of individual fibres average out so that the global structural stiffness remains largely unaffected [2, 8]. In contrast, systematic fibre misalignment typically occurs in form of localised, constant fibre angle deviations resulting in more severe effects and mostly arises during the manufacturing process. Possible sources include, but are not limited to, the end effector characteristics and control, distortion of textiles due to handling, ply movement after placement and complex geometries [2, 6].

Expectable fibre misalignment angles vary based on the aforementioned sources and depend heavily on the properties of the structure as well as the manufacturing process. In case of rotor blades, the geometry alone can cause fibre misalignment angles of up to 5° while angles in critical areas may exceed 10° [2]. Although it is not possible to determine a generally valid maximum tolerable fibre misalignment angle, values available in published studies may be used as rough references, e.g. ±2° [9] or ±5° [10].

10.1016/j.procir.2023.06.144

Studies investigating the effects of fibre misalignment on mechanical properties such as strength [7, 11], different moduli [7], and other properties [2, 7] have already been conducted, however, curvature is often disregarded or the structures are too specific for general effects to be derived. Therefore, the aim of this paper is to obtain an understanding regarding the effects of fibre misalignment on mechanical properties, specifically the stability, of double-curved, unidirectional plies and the correlations with other geometric quantities. Consequently, the results of this paper provide a foundation for extending the investigation to laminates based on which guidelines can be deduced for optimising the manufacturing process and design. By monitoring the resulting implications and feeding the information back to the structural design, the guidelines can be verified.

Effects of fibre misalignment are investigated numerically using a parametric finite element model. Fibre angles are assumed to be constant and represent extreme scenarios. Critical buckling stresses are obtained for various geometric configurations with parameter ranges deduced from the design of rotor blades and are subsequently analysed.

2. Finite element model

The numerical analysis is conducted using the solver *ABAQUS/Standard*. The double-curved ply of thickness t is generated by sweeping a curved profile of length w and curvature κ_w along a curved path of length l and curvature κ_l, as depicted in Fig. 1 (curvatures are substituted by their inverse, i.e. the radii of curvature, r_w and r_l, respectively). Material properties are summarised in Table 1. An edge load acting normal and tangential to the sweep path is applied to one edge, which is otherwise fixed. The opposite edge is fully clamped while the side edges are simply supported, see Fig. 1. Boundary conditions are expressed in terms of radial, tangential and meridional degrees of freedom in local coordinate systems. The critical buckling stress corresponding to the first buckling mode, σ_{cr}, is obtained through a linear eigenvalue prediction. Based on a convergence study performed on one of the configurations presented in section 3, the model is discretised by conventional shell elements S8R5 with an approximate size of 5 % of the shorter of the two lengths l and w, denoted by l_s. Validation of the model is achieved by comparing the total axial load required for displacing a cylindrical panel containing a circular hole by a given amount as well as the critical loads corresponding to the first five buckling modes against reference values available in the *ABAQUS* documentation [13] (the results deviate by less than 0.2 %).

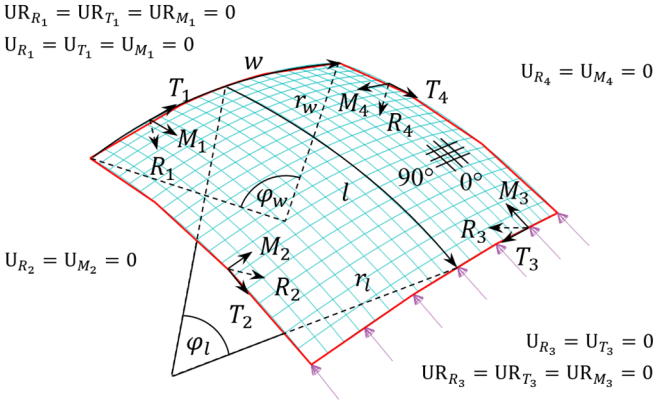

Fig. 1. Boundary conditions, loading and geometric parameters of the parametric finite element model.

Table 1. Material properties of transversely isotropic AS4/3501-6 [12].

Property	Value	Unit
Longitudinal modulus, E_1	126000	MPa
Transverse modulus, E_2	11000	MPa
In-plane shear modulus, G_{12}	6600	MPa
Through-thickness shear modulus, G_{23}	3618	MPa
In-plane Poisson's ratio, ν_{12}	0.28	-
Through-thickness Poisson's ratio, ν_{23}	0.52	-

Instead of the aforementioned parameters, geometric ratios are varied in the subsequent section. This is due to the fact that the critical buckling stress is independent of nominal values as long as the geometric ratios remain constant, consequently allowing sizing. Four ratios are required in order to fully describe the geometric properties of a double-curved shell. The first two, φ_l and φ_w, correspond to the angles covered by the sweep path and profile, respectively, see Fig. 1. The other two are the aspect ratio, α, and length-to-thickness ratio, β:

$$\alpha = \frac{l}{w}\,, \quad \beta = \frac{l_s}{t}\,, \quad \varphi_i = i\kappa_i = \frac{i}{r_i} \quad i \in \{l,\mathrm{w}\}$$

3. Results

The numerical test program is conducted in three blocks, namely B1, B2 and B3. The first block acts as a baseline and represents the case of a uniformly curved, quadratic ply implying $\kappa_l = \kappa_w$, $\alpha = 1$ and consequently $\varphi_l = \varphi_w = \varphi$. Therefore, the entire geometry is solely described by the ratios φ and β. Based on a reference configuration from B1, the initially assumed constant ratio α is varied in B2 while the assumption of a uniform curvature is kept. In B3, a quadratic ply with varying curvature in load direction is investigated based on the same reference configuration. Table 2 provides a summary of the analysed configurations. The test blocks are first analysed assuming curvatures of the same sign and subsequently repeated for opposite signs since both variations occur in the design of rotor blades.

The critical buckling stress is depicted as a function of the fibre angle, θ, and as absolute percent of the reference stress under $\theta = 0°$, see Fig. 1. Nominal stresses are provided in the respective figure captions. If not otherwise indicated, stresses are considered compressive. The data markers are colour-coded and refer to the number of halve waves (HW) present in the respective buckling shape. Half waves with a displacement magnitude of less than 25 % of the maximum displacement are not included.

Table 2. Geometric configurations of test blocks B1, B2 and B3.

Block	φ_l / °	φ_w / °	α	β
B1	{0, 10, 20, 30}	φ_l	1	{25, 50, 100}
B2	Depends on α	Depends on α	$\{0.\bar{3}, 0.5, 1, 2, 3\}$	50
B3	{0, 10, 20, 30}	10	1	50

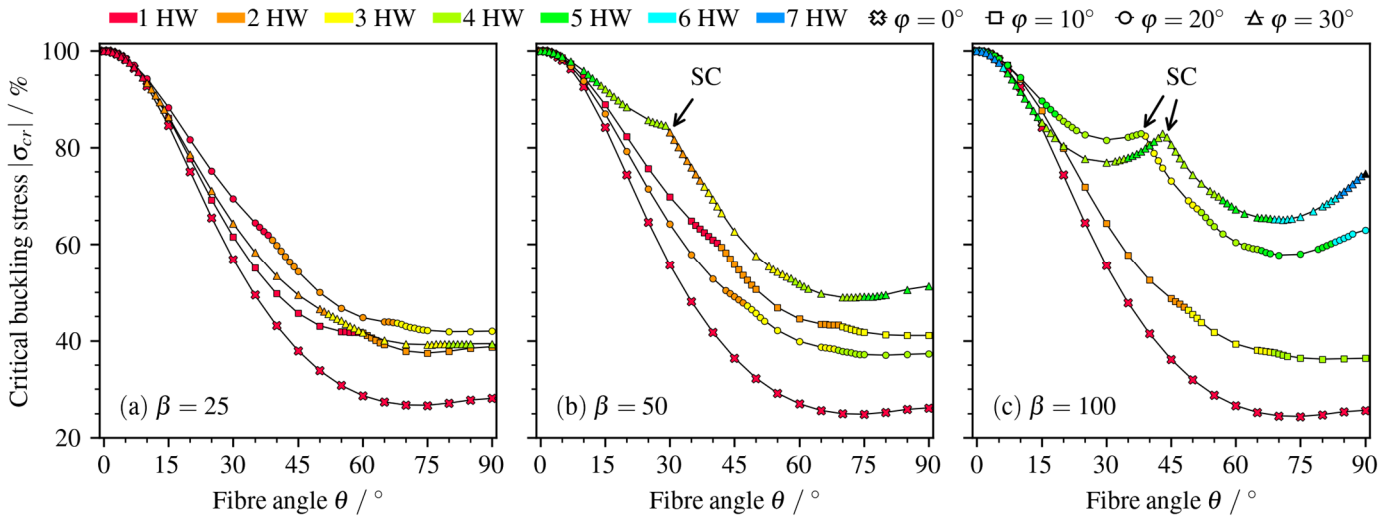

Fig. 2. Critical buckling stresses of B1 configurations with curvatures of same sign for various curvatures and length-to-thickness ratios (a-c); half wave (HW), sign change (SC); $\sigma_{cr}(\theta = 0°)$: 612 MPa ($\varphi = 0°$), 698 MPa ($\varphi = 10°$), 965 MPa ($\varphi = 20°$), 1376 MPa ($\varphi = 30°$) for $\beta = 25$; 170 MPa ($\varphi = 0°$), 256 MPa ($\varphi = 10°$), 471 MPa ($\varphi = 20°$), 480 MPa ($\varphi = 30°$) for $\beta = 50$; 44 MPa ($\varphi = 0°$), 122 MPa ($\varphi = 10°$), 128 MPa ($\varphi = 20°$), 154 MPa ($\varphi = 30°$) for $\beta = 100$.

3.1. Curvatures of same sign

The results obtained for the configurations of B1 are depicted in Fig. 2. The first thing to notice is that regardless of the fibre angle and length-to-thickness ratio, the percental buckling stresses (hereafter abbreviated as PBS) of all curved plies are higher than the respective reference PBS of the flat plies, the only exception being the configuration corresponding to $\beta = 100$ and $\varphi = 30°$ up to an angle of $\theta = 13°$. Contrary to implication, PBS do not necessarily increase with increasing curvature. A unique characteristic of the flat plies is that their buckling shapes consist of merely one half wave throughout all fibre angles. In contrast, the number of half waves in curved plies tends to increase with increasing curvature and length-to-thickness ratio. In fact, the only time the number of half waves can decrease with increasing fibre angle occurs during a sign change (SC), i.e. when the compressive edge load becomes tensile or vice versa. Sign changes observed for the configuration of $\beta = 100$ occur at $\theta = 39°$ and $\theta = 44°$, respectively, while that of $\beta = 50$ occurs at $\theta = 30°$. In all three cases, buckling up until the sign change is initiated by a tensile edge load, which then becomes compressive. A general characteristic observed for the curved plies are irregularities in the vicinity of buckling shape transitions indicated by comparatively rapid, localised changes of the gradient. This behaviour is sometimes accompanied by the occurrence of inflection points, e.g. around $\theta = 70°$ of the curve corresponding to $\beta = 50$ and $\varphi = 10°$. Buckling shape transitions tend to become more pronounced the smaller the number of half waves and the shorter the angular interval over which the transition occurs. The buckling shape transitions caused by a sign change of the edge load constitute extreme cases and highlight the effect of abrupt transitions as is exemplarily shown in Fig. 3. Towards $\theta = 90°$, all curves experience increasing PBS starting between $\theta = 70°$ and $\theta = 85°$. It is interesting to note that at $\theta = 90°$, the ply of highest curvature and length-to-thickness ratio is able to carry roughly 75 % of the reference stress before buckling while merely 25 % are achieved without curvature. In the range of realistic fibre misalignment angles, no significant qualitative differences are observable with PBS of 91-96 % at $\theta = 10°$.

Based on the ply configuration $\varphi = 10°$ and $\beta = 50$ from B1, the aspect ratio is varied in B2 as shown in Fig. 4. Plies with $\alpha = 1/3$ and $\alpha = 1/2$ exhibit a similar behaviour as the

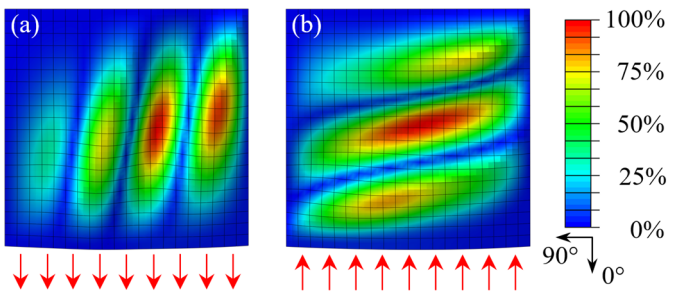

Fig. 3. Total displacement magnitude of the buckling shapes corresponding to $\varphi = 20°$ and $\beta = 100$ from B1 with curvatures of the same sign at (a) $\theta = 38°$ and (b) $\theta = 39°$; boundary conditions are omitted for simplicity.

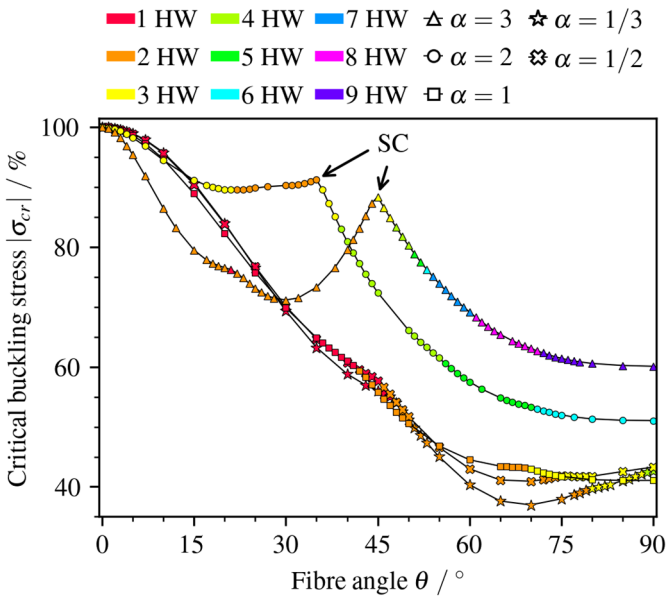

Fig. 4. Critical buckling stresses of B2 configurations with curvatures of same sign for various aspect ratios; half wave (HW), sign change (SC); $\sigma_{cr}(\theta = 0°)$: 196 MPa ($\alpha = 1/3$), 205 MPa ($\alpha = 1/2$), 256 MPa ($\alpha = 1$), 190 MPa ($\alpha = 2$), 159 MPa ($\alpha = 3$).

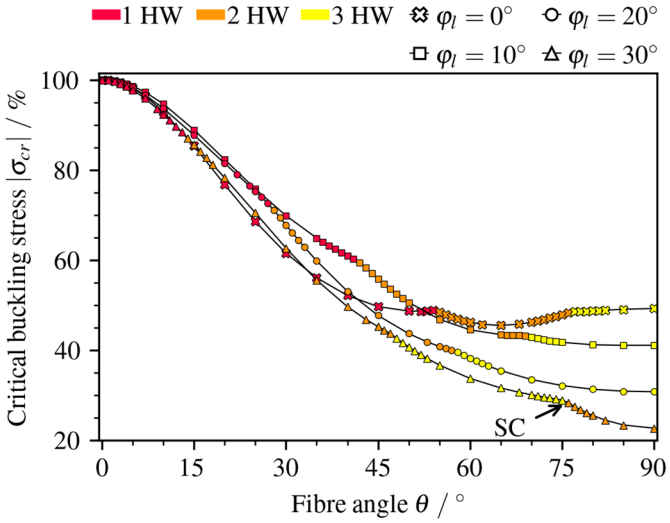

Fig. 5. Critical buckling stresses of B3 configurations with curvatures of same sign for various curvatures; half wave (HW), sign change (SC); $\sigma_{cr}(\theta = 0°)$: 191 MPa ($\varphi_l = 0°$), 256 MPa ($\varphi_l = 10°$), 395 MPa ($\varphi_l = 20°$), 535 MPa ($\varphi_l = 30°$).

quadratic ply from which they deviate less than 6 % and 3 %, respectively. Further similarities include the number of half waves and angular intervals in which the buckling shape transitions occur. In contrast, plies with $\alpha > 1$ show a significantly different buckling behaviour. Firstly, the number of half waves at $\theta = 0°$ is greater than one and the number of buckling shape transitions is increased. In addition, the critical buckling stress is initially tensile and becomes compressive at $\theta = 36°$ and $\theta = 45°$, respectively. All plies behave relatively similar in the realistic range of fibre misalignment angles and reach PBS of 94-96 % at $\theta = 10°$, except for the one with $\alpha = 3$, which rapidly drops to just 87 %.

Based on the same reference configuration as used in B2, different curvature combinations are investigated in B3, see Fig. 5. Overall, the results show mostly minor qualitative differences between the configurations. For instance, with increasing fibre angle and curvature, the number of half waves increases, starting with one half wave at $\theta = 0°$ for all configurations. In addition, PBS at $\theta = 90°$ vary due to different gradients and decrease from 49 % to 23 % with increasing curvature. A significant difference in behaviour between the ply of highest curvature and the other configurations is the sign change from a compressive to a tensile stress at $\theta = 76°$. In the range of realistic fibre misalignment angles, PBS of 92-95 % are present at $\theta = 10°$. In general, the same irregularities as described for B1 are observable in the buckling shape transition intervals of B3 as well as B2.

3.2. Curvatures of opposite sign

Repeating the analyses of B1 with curvatures of opposite sign yields the results depicted in Fig. 6. As before, the number of half waves tends to increase with increasing fibre angle and curvature. The irregularities occurring during the buckling shape transitions are also present. The qualitative behaviour among curved plies is similar but differs compared to the flat ply. This observation becomes more obvious with increasing length-to-thickness ratio. In case of $\beta = 100$ for example, an increase of curvature from 0° to 10° influences the buckling behaviour more severely than an increase from 10° to 30°. In contrast to the results obtained for curvatures of the same sign, there are no sign changes of the compressive edge load. Nevertheless, the number of half waves can decrease with increasing fibre angle. In addition, the PBS at $\theta = 90°$ are generally higher and increase with increasing curvature and length-to-thickness ratio. In the range of realistic fibre misalignment angles, PBS of 89-94 % are reached at $\theta = 10°$.

The results obtained for the configurations of B2 with opposite sign are depicted in Fig. 7. The initial behaviour is qualitatively similar up to roughly $\theta = 20°$ regardless of the aspect ratio. However, for increasing fibre angles, clear distinctions are present between $\alpha > 1$, $\alpha = 1$ and $\alpha < 1$. While the plies of the latter ratio exhibit constantly decreasing PBS, which deviate by less than 4 %, up to 25 % and 28 %, respectively, those of the former reach minimum values around $\theta = 45°$ followed by an increase up to 83 % and 94 %, respectively. Meanwhile, the quadratic ply shows a mixture of the aforementioned characteristics. Contrarily to the

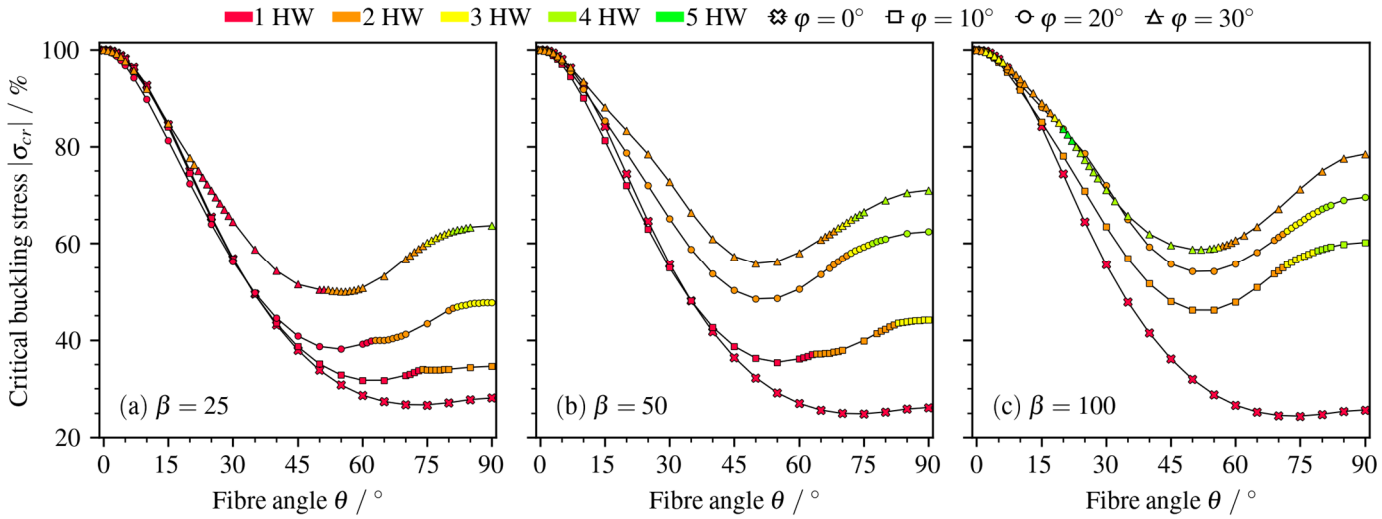

Fig. 6. Critical buckling stresses of B1 configurations with curvatures of opposite sign for various curvatures and length-to-thickness ratios (a-c); half wave (HW); $\sigma_{cr}(\theta = 0°)$: 612 MPa ($\varphi = 0°$), 640 MPa ($\varphi = 10°$), 715 MPa ($\varphi = 20°$), 690 MPa ($\varphi = 30°$) for $\beta = 25$; 170 MPa ($\varphi = 0°$), 200 MPa ($\varphi = 10°$), 205 MPa ($\varphi = 20°$), 206 MPa ($\varphi = 30°$) for $\beta = 50$; 44 MPa ($\varphi = 0°$), 54 MPa ($\varphi = 10°$), 62 MPa ($\varphi = 20°$), 73 MPa ($\varphi = 30°$) for $\beta = 100$.

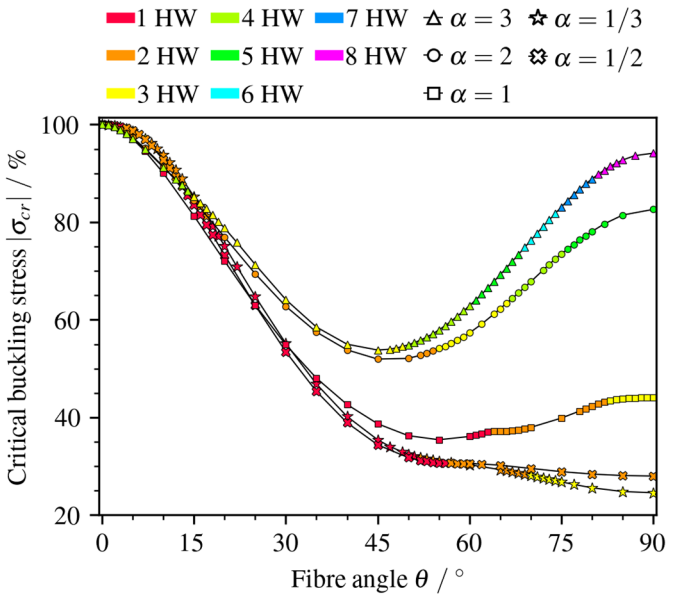

Fig. 7. Critical buckling stresses of B2 configurations with curvatures of opposite sign for various aspect ratios; half wave (HW); $\sigma_{cr}(\theta = 0°)$: 172 MPa ($\alpha = 1/3$), 178 MPa ($\alpha = 1/2$), 200 MPa ($\alpha = 1$), 96 MPa ($\alpha = 2$), 82 MPa ($\alpha = 3$).

configurations with curvatures of same sign, the number of half waves can decrease with increasing fibre angle. Irregularities in the buckling shape transitions are less pronounced, especially for a high number of half waves. PBS of 90-94 % are achieved in the range of realistic fibre misalignment angles at $\theta = 10°$.

Fig. 8 depicts the results obtained for different curvature combinations. Compared to the configurations with curvatures of the same sign, the gradients of PBS curves for the double-curved plies are initially steeper and become positive towards $\theta = 90°$. The single-curved ply, i.e. $\varphi_l = 0°$, which constitutes a cylindrical panel, exhibits the highest PBS throughout all fibre angles. Buckling shape transitions occur at relatively high fibre angles with irregularities becoming less pronounced with increasing curvature. Regarding the realistic range of fibre misalignment angles, PBS of 88-93 % are achieved.

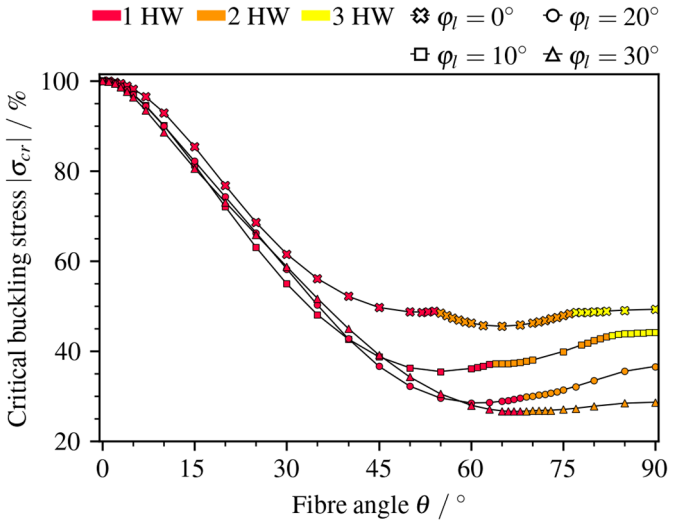

Fig. 8. Critical buckling stresses of B3 configurations with curvatures of opposite sign for various curvatures; half wave (HW); $\sigma_{cr}(\theta = 0°)$: 191 MPa ($\varphi_l = 0°$), 200 MPa ($\varphi_l = 10°$), 233 MPa ($\varphi_l = 20°$), 257 MPa ($\varphi_l = 30°$).

4. Discussion

Regarding fibre misalignment angles of up to $\theta = 10°$, which are relevant for practical applications, any of the previously analysed geometric ratios seems to have minor effects on the percental buckling stress as indicated by the initially similar behaviours of the analysed configurations. Small gradients near $\theta = 0°$ allow for relatively high tolerances before the buckling stress drops significantly. For example, 95 % of the reference buckling stress are on average achieved at fibre angles of $\theta = 8.9°$ and $\theta = 7.6°$ for curvatures of the same and opposite sign, respectively. For comparison, 90 % are on average achieved at $\theta = 13.3°$ and $\theta = 11.3°$. Although the percental buckling stress exhibits weak dependencies on the geometric ratios, the nominal values are greatly affected. The highest critical buckling stress (1376 MPa) is obtained for the configuration of $\beta = 25$, $\varphi = 30°$ and curvatures of the same sign while the lowest (44 MPa) is obtained for $\beta = 100$ and $\varphi = 0°$, both from the first test block. This leads to the conclusion that the critical buckling stress can be maximised by increasing the curvature and reducing the length-to-thickness ratio, the latter of which is already known from buckling of flat plates. The results of the other test blocks indicate that the buckling stress can be further increased by having curvatures of the same sign and an aspect ratio of $\alpha = 1$, although the ideal aspect ratio probably depends on the combination of boundary conditions and should be analysed in more detail.

The increase of buckling stress with increasing ply curvature is most likely attributed to the fact that an emerging half wave has a curvature of its own and achieving compatibility between the two curvatures requires larger strains for increasing ply curvature, thus resulting in higher stresses. Furthermore, an increasing length-to-thickness ratio negatively influences the buckling stiffness of the ply, hence explaining the resulting decrease of the critical buckling stress. Buckling due to a tensile edge load occurs when the compressive stresses resulting from the Poisson effect encounter a significantly lower stiffness than stresses resulting from a compressive edge load would. This thesis is supported by the fact that the buckling stresses of the B1 configurations exhibiting a sign change become compressive for increasing fibre angles, i.e. decreasing stiffness in load direction. The cause for the increase of buckling stress towards $\theta = 90°$ is likely found in the biaxial state of stress. While buckling for intermediate fibre angles occurs due to a combination of stresses resulting from the edge load and the Poisson effect, a fibre angle of $\theta = 90°$ leads to a high stiffness in the direction perpendicular to the edge load, thereby effectively reducing the biaxial state of stress to a unidirectional one. The irregularities occurring during buckling shape transitions result most likely due to the fact that each buckling shape has its own function relating the buckling stress to the fibre angle. Since the functions are offset from one another and the analysed buckling stress is only evaluated for the first buckling mode, the buckling shape transitions coincide with the intersections of the buckling shape functions. On the one hand, sign changes exhibit abrupt transitions with visible peaks between buckling shapes as can be seen in Fig. 2, Fig. 3

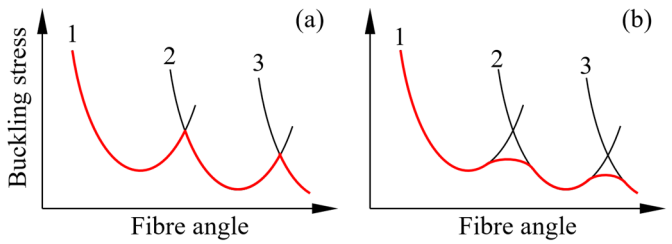

Fig. 9. Transition of lowest buckling mode between buckling shapes 1-3: (a) abrupt change at intersection; (b) transition over a longer angular interval.

and as illustrated in Fig. 9 (a). On the other hand, regular buckling shapes transition over a small interval, which has a smoothing effect as exaggeratedly shown in Fig. 9 (b). Buckling shape transitions becoming less pronounced for increasing curvature and number of half waves would imply that the offsets between the individual shape functions decrease and/or that the shape functions stretch. A consequence of the buckling shape transitions is that a ply with increasing curvature does not automatically result in higher percental buckling stresses as can be seen exemplarily for the configurations of $\varphi = 10°$ and $\varphi = 30°$ with $\beta = 25$ at $\theta \approx 60°$ in Fig. 2.

5. Conclusion

General effects of fibre misalignment on the stability of double-curved, unidirectional plies as well as correlations with other geometric parameters are analysed using a parametric finite element model. In the range of realistic fibre misalignment angles, merely weak dependencies are found for the percental buckling stress, however, nominal values are greatly affected. Therein, the critical buckling stress tends to increase with increasing curvature and decreasing length-to-thickness ratio. The former effect is intensified by having curvatures of the same sign. The ideal aspect ratio likely depends on the combination of boundary conditions and should be investigated further. Small gradients in the vicinity of perfectly aligned fibres allow for relatively large fibre angle tolerances, e.g. 95 % of the reference buckling stress are on average achieved at fibre misalignment angles of 8.9° for curvatures of the same sign.

Further phenomena observed from the results of the numerical test program include a tendency for the number of half waves to increase with increasing fibre angle, curvature and length-to-thickness ratio. Transitions between buckling shapes cause irregularities in the course of buckling stresses, which become more pronounced the smaller the number of half waves and the shorter the angular interval over which the transitions occur. Furthermore, buckling under tensile loads can occur when compressive stresses resulting from the Poisson effect encounter a comparatively low stiffness.

Before extending the investigation to laminates, it could be beneficial to conduct complementary, non-linear buckling analyses using the Riks method in order to verify the herein presented results. In addition, a detailed design of experiments and a significance analysis could be performed to better understand the correlations between the parameters.

Acknowledgements

The authors would like to thank the federal state of Lower Saxony and the European Regional Development Fund (ERDF) for financial and organizational support of the project AutoBLADE.

References

[1] Ohlendorf J-H, Richrath M, Franke J, Brink M, Thoben K-D. Towards automation of wind energy rotor blade production: a review of challenges and application examples. *Advanced Manufacturing: Polymer and Composites Science*; 6:4; p. 173-190; 2020

[2] VanSkike WP, Hale RD. Effects of fiber misalignment on composite wind turbine rotor blades. *AIAA SciTech Forum*, Grapevine, Texas, 9-13 January; 2017

[3] Yurgartis SW. Measurement of small angle fiber misalignments in continuous fiber composites. *Composites Science and Technology*; 30:4; p. 279-293; 1987

[4] Raimondi L, Brugo TM, Zucchelli A. Fiber misalignment analysis in PCM-UD composite materials by full field nodal method. *Composites Part C: Open Access*; 5; 2021

[5] Mesogitis TS, Skordos AA, Long AC. Stochastic simulation of the influence of fibre path variability on the formation of residual stress and shape distortion. *Polymer Composites*; 38:12; p. 2642-2652; 2017

[6] Pagani A, Sanchez-Majano AR. Stochastic stress analysis and failure onset of variable angle tow laminates affected by spatial fibre variations. *Composites Part C*: Open Access; 4; 2021

[7] Bednarcyk BA, Aboudi J, Arnold SM. The effect of general statistical fiber misalignment on predicted damage initiation in composites. *Composites: Part B*; 66; p. 97-108; 2014

[8] Potter K, Khan B, Wisnom M, Bell T, Stevens J. Variability, fibre waviness and misalignment in the determination of the properties of composite materials and structures. *Composites: Part A*; 39; p. 1343-1354; 2008

[9] Khakimova R, Zimmermann R, Burau F, Siebert M, Arbelo M, Castro S, Degenhardt R. Optimization of the manufacturing process of conical shell structures using prepreg laminates. *13th European Conf. on Spacecraft Structures, Materials & Environmental Testing*, Braunschweig, Germany, 1-4 April; 2014

[10] Gerngross T, Nieberl D. Automated manufacturing of large, three-dimensional CFRP parts from dry textiles. *CEAS Aeronautical Journal*; 7; p. 241-257; 2016

[11] Kawai M, Yajima S, Hachinohe A, Takano Y. Off-axis fatigue behavior of unidirectional carbon fiber-reinforced composites at room and high temperatures. *Journal of Composite Materials*; 35:7; 2001

[12] Kaddour AS, Hinton MJ, Li S, Smith PA. The world-wide failure exercises: how can composites design and manufacture communities build their strength. *16th European Conference on Composite Materials*, Sevilla, Spain, 22-26 June; 2014

[13] ABAQUS 2020 documentation; *Laminated composite shells: buckling of a cylindrical panel with a circular hole*